1-1-2015

Ultrafast spin polarization in a multiferroic manganite BiFe0.5Mn0.5O3 thin film

Zeyu Zhang
Shanghai University

Zuanming Jin
Shanghai University

Xian Lin
Shanghai University

Zhenxiang Cheng
University of Wollongong, cheng@uow.edu.au

H Y. Zhao
Wuhan Institute of Technology

See next page for additional authors

Ultrafast spin polarization in a multiferroic manganite BiFe0.5Mn0.5O3 thin film

Abstract

In this work, we present observations of ultrafast carrier dynamics and spin polarization in a multiferroic manganite BiFe0.5Mn0.5O3 film excited by linearly and circularly polarized femtosecond pulses, respectively. The d-band charge transfer transition is reasonably assigned to Γ3 → Γ5. The transient reflectivity decay on a time scale as fast as only 0.3 ps is consistent with the picture of ultrafast electron-phonon coupling. The ultrafast switching of polarization ellipticity (< 150 fs) originates from a transient coherent spin polarization by optical orientation. The ultrafast spin polarization switching is assigned to the Raman coherence process.

Keywords

thin, 5o3, bife0, film, polarization, spin, ultrafast, manganite, 5mn0, multiferroic

Disciplines

Engineering | Physical Sciences and Mathematics

Publication Details

Zhang, Z. Y., Jin, Z. M., Lin, X., Cheng, Z. X., Zhao, H. Y., Kimura, H. & Ma, G. H. (2015). Ultrafast spin polarization in a multiferroic manganite BiFe0.5Mn0.5O3 thin film. Europhysics Letters: a letters journal exploring the frontiers of physics, 112 (3), 37007-1-37007-5.

Authors

Zeyu Zhang, Zuanming Jin, Xian Lin, Zhenxiang Cheng, H Y. Zhao, Hideo Kimura, and Guohong Ma

Originally published as “Ultrafast spin polarization in a multiferroic manganite

BiFe0.5Mn0.5O3 thin film”

Ultrafast spin-ordering in a multiferroic manganite Bi_2FeMnO_6 thin film

Zeyu Zhang[1], Zuanming Jin[1], Xian Lin[1], Zhenxiang Cheng[2], Hongyang Zhao[3], and Hideo Kimura[3], Guohong Ma[1]

[1] *Department of Physics, Shanghai University, 99 Shangda Road, Shanghai 200444, P. R. China*

[2] *Institute for Superconductor and Electronic Materials, University of Wollongong, Squair Ways, North Wollongong, NSW 2500, Australia*

[3] *National Institute for Materials Science, Sengen 1-2-1, Tsukuba, Ibaraki 305-0047, Japan*

In this work, we present the observation of ultrafast carrier dynamics and spin ordering in the multiferroic manganite Bi_2FeMnO_6 (BFMO) film excited by linearly and circularly polarized femtosecond pulses, respectively. The d-band charge transfer transition is reasonably assigned to $\Gamma_3 \rightarrow \Gamma_5$. The photo-excited carriers relax firstly within around 0.3 ps, corresponding to the electron-phonon coupling. The ultrafast switching of polarization ellipticity (<150 fs) is originated from a transient coherent spin ordering by optical orientation, which is assigned to Raman coherence process.

Multiferroic materials, which show the simultaneous coexistence of ferroelectric and magnetic phases, have attracted extensive attention in the past decades [1-3]. By doping another magnetic transition metal cation on the B-site in an ABO_3 perovskites oxide, $Bi_2BB'O_6$, can provide ferromagnetic exchange according to the Goodenough-Kanamori's rules [4]. Multiferroic manganite Bi_2FeMnO_6 (BFMO), a compound of $BiFeO_3$ and $BiMnO_3$, has been recently designed theoretically and fabricated experimentally. More intense research has resulted in promising findings such as multiferroic, coexisting a small net ferromagnetic magnetization at room temperature and ferroelectricity at low-temperature in BFMO [5-7]. In the previous work, based on the small magnetic moment observed in M-H loop, Mn-O-Mn is antiferromagnetically ordered in BFMO, which is much weaker than Fe-O-Fe ordering [8]. It is important to note, the desired electronic configuration of B-B' cation is difficult to be obtained, owing to the mixed valence states. Furthermore, long-range ferromagnetism requires alternation B-B' cation ordering along the fundamental perovskite directions [4].

Femtosecond optical *pump* pulse has been widely used to suddenly create a nonequilibrium state in the semiconductors [9,10] and ferromagnetic materials [11,12]. The subsequent *electron* and/or *spin* relaxation dynamics is measured by time-delayed *probe* pulse. Based on the transfer of angular momentum from circularly polarized light to the medium, a nonequilibrium electron polarization was created in antiferromagnetic Mott insulators [13], topological insulator [14] and also paramagnetic crystal [15], which has been ascribed to a transient spin polarization

with fast depolarization. Less studied and very interesting material system is the case of multiferroics, which are generally classified to the strongly correlated electrons system, combining both magnetic- and semiconducting-properties. In recent years, optical pump-probe spectroscopy has been employed as a crucial alternative tool for investigating the strong coupling between spin, charge, and lattice on different time scales in multiferroic systems [16-20]. In addition, the individual degree of freedom is sensitive to various optical characterization of probe pulse, such as absorption, reflection or polarization. The present work is motivated by uncovering the question that is it possible to generate a coherent transient spin ordering in a multiferroic system by using the ultrashort laser pulse?

A well-crystallized single-phase BFMO film was deposited on a silicon substrate using a pulsed laser deposition method (PLD) at 923 K with 500 - 600 mTorr dynamic oxygen. The film thickness is about 150 nm. The time-resolved pump-probe study of BFMO film was measured with a standard reflection-geometry. The light source was provided by a commercial mode-locked Ti:sapphire laser (Spitfire Pro, Spectra-Physics) running at the repetition rate of 1 kHz, the pulse width of 120 fs. A quarter wave plate was placed in the pump path, which enables the tuning of the pump pulse helicity between right- and left- circularly polarized states with its fast axis at an angle Φ to the plane of incident pump beam. Both of the pump and probe beams were focused on the surface of the sample with a spot diameter about 200 μm. The fluence of the probe beam was weaker than that of the pump beam at least a factor of ten. The BFMO film under investigation were photo-excited at 800 nm (1.55 eV). The

penetration length is 100 nm, which is much less than the thickness of the film under investigation here. Lock-in amplifier detection was used to record pump-induced relative change in reflected probe power as function of pump-probe delay time. In addition, a Glan prism and balanced optical bridge was used to detect the pump-induced transient polarization rotation or ellipticity change of the linearly polarized probe beam. In our measurements, the sample was mounted in a closed-cycle liquid-He cryostat in vacuum chamber with four optically accessible windows, which is allowed control of the sample temperature in a range of 100 - 300 K.

Figure 1 (a) shows the typical time-resolved transient reflectivity ($\Delta R/R$) of BFMO film, which was measured with a pump fluence of 500 $\mu J/cm^2$ at 120 K, also as a proof of the high quality of the BFMO film. During or immediately following the pulse, the $\Delta R/R$ starts rising sharply (population) and then decays by a non-radiative double exponential relaxation process. The fast and slow exponential decays mostly arise from the isotropic relaxations of non-equilibrium electron and lattice systems. We will find in the following that the electron dynamics takes place essentially slower than the coherent spin dynamics.

The photo-induced change of complex dielectric susceptibility driven by linearly- and circularly-polarized pump pulses are corresponding to linear- and circular anisotropy, respectively [21]. The *antisymmetric* nonlinear perturbation of the dielectric permittivity tensor is deduced from the pump-induced magneto-optical Kerr effect. The ellipticity signal relates to $f(N) \cdot \boldsymbol{M}$, where $\boldsymbol{M}$ is the magnetization, and f

(*N*) is determined by the complex refractive index *N* at the probe frequency. We can find the direct proportion relation between the $\boldsymbol{M}$ and the magnitude of the Gaussian-like peak in the ellipticity signal [9]. The *symmetric* nonlinear perturbation of the dielectric permittivity is deduced from the rotation of the probe polarization plane, which is due to the nonmagnetic, third-order nonlinear optical Kerr effect. Attention should be paid that only the off-diagonal elements of the complex dielectric susceptibility tensor is related to spin-based phenomenon, which could be classified as optical orientation (resonant case) [13] and inverse Faraday effect (off-resonant case) [12,15].

Typical temporal behaviors of the photo-induced polarization ellipticity of the reflected probe pulse ($\Delta\eta^{K}$) are shown in Fig. 1 (b), measured at room temperature, in which the excitations with linearly, left- and right-circularly (σ_- and σ_+) polarized pump beams are used under pump fluence of 8 mJ/cm^2 and wavelength of 800 nm. A direct comparison of time-resolved reflectivity and polarization ellipticity of the probe pulses is performed to access the complete transient photo-induced phenomena in the sample. In contrast to the photo-induced reflectivity with a multi-exponential decay, the initial impression of the dynamical response $\Delta\eta^{K}_{\sigma+(-)}$ is a two-step recovery, which can be decomposed into a symmetric Gaussian peak and a relaxing slope. This striking difference in temporal profiles demonstrates a separate physical origin between the measured $\Delta\eta$ and $\Delta R/R$ response. We note that the Gaussian-like peak of $\Delta\eta^{K}_{\sigma+(-)}$ remembers the polarization of pump pulse, it clearly change sign when the helicity of the pump pulses is reversed. Moreover, $\Delta\eta^{K}_{\sigma+(-)}$ is maximum as the pump

and probe beams are overlapped temporally. On the other hand, the measured slower relaxation slope is independent on the helicity of the pump pulse, which can also be induced by linearly polarized pump beam. This suggests that the temporal relaxation slope can be assigned to the heat-induced birefringence, driven by the dynamical phenomena involving phonons. This temporal birefringence dominates the isotropic changes in the refractive index.

As shown in Fig. 2 (a), the differential transient polarization ellipticity $\Delta\eta^K = 1/2(\Delta\eta^K{}_{\sigma+} - \Delta\eta^K{}_{\sigma-})$ (red squares) between the σ_+ and σ_- pump beam allows us to minimize the thermal effect as the primary source of the net dichroism excited by the pump beam. In the following, we attribute this to the pure magnetic-order contribution. Figure 2 (b) shows the differential polarization rotation $\Delta\theta^K = 1/2(\Delta\theta^K{}_{\sigma+} - \Delta\theta^K{}_{\sigma-})$ (black circles), excited with opposite circularly polarized pulses. Notice that the differential polarization ellipticity shows almost a Gaussian shape, while the differential polarization rotation follows a derivative shape of the ellipticity counterpart. They are related through the Kramers-Kronig relation [14].

In Fig. 3 (a), we present the measured peak amplitude of $\Delta\eta^K$ as a function of the temperature (red squares) pumped by circular polarized pulse. It is important to see that the transient $\Delta\eta^K$ follows the same trend of the static magnetization curve (green circles) of the sample with decreasing the temperature. The increase of magnetization is due to the increasing the long-range magnetic-order contribution [8], that occurs as the sample cools down. Base on the similar temperature dependence, it is reasonable to purports the spin origin of the observed transient photo-induced anisotropy signal.

It is instructive to compare the results on the ultrafast photo-induced anisotropy for different polarization of the pump pulse. The Fig.3 (b) shows the dependence of the peak amplitude of $\Delta\eta^K$ (black circles) upon the orientation of the fast axis of the quarter-wave plate relative to the polarization of the incident pump pulse, i.e., the helicity of the pump pulse. The dependence can be well reproduced by a sum of twofold (blue dashed line) and fourfold (red dotted line) sinusoidal functions, which come from two main contributions: the spin-related *optical orientation* and nonmagnetic, third-order nonlinear *optical Kerr effect* in the ultrafast time scale, respectively [22]. It can be found that the contribution from optical orientation is maximized while OKE vanishes when the pump beam is circularly polarized. Having noted that the Kerr ellipticity induced by spin ordering only appears in presence of the pump pulse.

It has been reported that the time scale of spin orientation can be extract by a simple model, which had been adapted firstly for conventional GaAs [23] and then oxide insulators [13]. Under the assumption that both pump and probe pulses have Gaussian temporal profiles, the photo-induced polarization rotation and ellipticity can be well fitted by: $\theta + i\epsilon = A\exp\left(-\frac{t^2}{4\omega^2}\right) + B\exp(\frac{\omega^2}{\tau_R^2} - \frac{t}{\tau_R}) \times \left[1 - \mathrm{erf}(\frac{\omega}{\tau_R} - \frac{t}{2\omega})\right]$, where t is the pump-probe time delay and ω= 120 fs is the width of pump pulse. The erf is the Gaussian error function. A and B correspond to the symmetric and antisymmetric of the dielectric susceptibility tensor ε. In the spin dynamics of semiconductor and ferromagnetic metals, the transient spin relaxation mechanism is generally consisted with the spin-orbital coupling [23]. Owing to the orbital

quenching in 3d electron materials, we take another spin relaxation process into account. A characteristic τ_R is Raman coherence time, which describes a transition in a degenerate state with symmetry $|+\rangle$ to $|-\rangle$ changing the magnetic quantum number and the magnetic polarization. As shown in Fig. 2(b), τ_R = 100 ± 30 fs extracted from the fitting is shorter than the laser pulse duration.

To understand the photo-induced charge- and spin-related response of BFMO, we need to consider the charge transfer (CT) transitions [24]. The band gap for $BiFe_xMn_{1-x}O_3$ could be modulated from 1.2 ~2.6 eV by altering the doping ratio x, between 0 and 1 [25]. Since the onset of the d-d CT transitions (~2 eV) in Fe^{3+}-based ferrites is strongly blue-shifted as compared to the Mn^{3+}-based manganite [24], and also the onset O-Mn, CT transition at higher energy (~ 5 eV), 1.55 eV pump and probe pulse used here is attributed to the intersite Mn^{3+} ion d-d transitions. The ground state of the 3d transition is formed by the oxygen 2*p* state strongly hybridized with the $3d_{3z^2-r^2}$ and $3d_{x^2-y^2}$ states. In the orthorhombic manganite BFMO, the ^5D is split into a $^5\Gamma^{3+}$ low state and a $^5\Gamma^{5+}$ high state under the influence of a moderated crystal field of the octahedral symmetry m3m [26]. Figure1 (c) shows a schematic energy-level diagram for the optical transition ($\Gamma^3 \rightarrow \Gamma^5$) between the hybridized O^{2-}(2p)-Mn^{3+}(3d) states and the Mn^{3+} states.

The fast decay of ΔR/R corresponds to the carriers leaving the excited high state Γ^5 via electron-phonon couplings, which is characterized by the population relaxation time $\tau_1 \approx 300$ fs. The following slow process could be contribute to the carrier recombination from the upper state to the Mn-O hybrid state. The amplitude and time

constant of the carrier relaxation dynamics is dependent on sample temperature. On the other hand, a circular pump pulse creates a coherent superposition of the excited states $|+\rangle$ and $|-\rangle$. Electric-dipole optical transitions from the ground state $\Gamma_3|g\rangle$ are allowed to the doubly degenerate state of symmetry state Γ_5. In the case of a circularly polarized pump pulse, it is convenient to use a circular basis for the wave functions of the doubly degenerate excited states $|+\rangle$ and $|-\rangle$, where the states $|\pm\rangle$ are characterized by the *z* projection J_z of the total angular momentum equal to ±1, respectively. The nonzero electric-dipole matrix elements for transitions from the ground state $|g\rangle$ to the excited state $|+\rangle$ and $|-\rangle$ are $\langle g|d^+|+\rangle = \langle g|d^-|-\rangle = d$, respectively. $|g\rangle, |+\rangle$ and $|-\rangle$ constitute a degenerate phenomenological three-level model, as shown in Fig. 1(c). The transitions between $|+\rangle$ and $|-\rangle$ are characterized by a coherence time τ_R = 100 ± 30 fs, which could be contributed to Raman coherence and demonstrates the relaxation time of angular momentum J_z. Furthermore, as shown in Fig. 3 (c), the peak magnitude of $\Delta\eta^K$ increases linearly with pump fluence, which means that the coherent superposition states is proportional to the intensity of the pump pulse, while the coherent time is independent on the pump fluence.

In summary, the ultrafast photo-induced spin ordering in the multiferroic Bi_2FeMnO_6 has been observed on a femtosecond time scale. By means of femtosecond pump-probe transient reflectivity, Kerr rotation and ellipticity measurement, two relaxation time are disclosed. By pulse pumping, the charge transfer carriers in BFMO leave the excited state at about 300 fs by electron-lattice coupling and then recombine. With circularly polarized pulse pumping, the helicity

dependent coherent spin ordering is observed. The spin polarization relaxation time is determined to be τ_R= 100 ± 30 fs, which is assigned to the Raman coherence process between the excited doubly degenerate state $\Gamma^5|+,-\rangle$ state. This study provides the experimental evidence to optical orientation in Bi_2FeMnO_6 regarding ultrafast photo-induced spin ordering and paves the way to a large application potential in future spin-based all-optical technologies.

Acknowledgements: The research is supported by National Natural Science Foundation of China (11174195), Ph.D. Programs Foundation of Ministry of Education of China (20123108110003) and the Research Innovation Fund of the Shanghai Education Committee (14ZZ101). Z. X. Cheng thanks Australia Research Council for support.

Reference

[1] M. Bibes, and A. Barthélémy, Nat. Mater. **7**, 425 (2008).

[2] W. Eerenstein, N. D. Mathur, and J. F. Scott, Nature **442**, 759 (2006).

[3] J. T. Heron, M. Trassin, K. Ashraf, M. Gajek, Q. He, S. Y. Yang, D. E. Nikonov, Y-H. Chu, S. Salahuddin, and R. Ramesh, Phys. Rev. Lett. **107**, 217202 (2011).

[4] J. Zhang, H. Li, Perovskite: Crystallography, Chemistry & Catalytic Performance, Nova Science Publishers Inc (2013).

[5] H. Zhao, H. Kimura, Z. Cheng, X. Wang, K. Ozawa, and T. Nishida, J. Appl. Phys. **108**, 093903 (2010).

[6] E.-M. Choi, S. Patnaik, E. Weal, S.-L. Sahonta, H. Wang, Z. Bi, J. Xiong, M. G. Blamire, Q. X. Jia and J. L. MacManus-Driscoll, Appl. Phys. Lett. **98**, 139903 (2011)

[7] L. Bi, A. R. Taussig, H. Kim, L. Wang, G. F. Dionne, D. Bono, K. Persson, G. Ceder, and C. A. Ross, Phys. Rev. B 78, 104106 (2008).

[8] Y. Du, Z. X. Cheng, S. X. Dou, X. L. Wang, H. Y. Zhao, and H. Kimura, Appl. Phys. Lett. **97**, 122502 (2010).

[9] H. Ma, Z. Jin, Z. Zhang, G. Ma, and L. Wang, AIP Advances **2**, 012116 (2012)

[10] J. Kim, X. Hong, C. Jin, SF. Shi, C-Y. S. Chang, M-H. Chiu, L-J. Li, F. Wang. Science, **346**, 1205 (2014).

[11] E. Beaurepaire, J.-C. Merle, A. Daunois, and J.-Y. Bigot, Phys. Rev. Lett. **76**, 4250 (1996).

[12] A. Kirilyuk, A. V. Kimel, and Th. Rasing, Rev. Mod. Phys. **82**, 2731 (2010).

[13] V. V. Pavlov, R. V. Pisarev, V. N. Gridnev, E. A. Zhukov, D. R. Yakovlev, and M. Bayer, Phys. Rev. Lett. **98**, 047403 (2007).

[14] F. Boschini, M. Mansurova, G. Mussler, J. Kampmeier, D. Grützmacher, L. Braun, F. Katmis, J. S. Moodera, C. Dallera, E. Carpene, C. Franz, M. Czerner, C. Heiliger, T. Kampfrath, M. Münzenberg, arXiv:1506.02692 (2015).

[15] Z. Jin, H. Ma, L. Wang, G. Ma, F. Guo and J. Chen, Appl. Phys. Lett. **96**, 201108 (2010).

[16] Z. Jin, H. Ma, G. Li, Y. Xu, G. Ma, and Z. Cheng, Appl. Phys. Lett. **100**, 021106 (2012).

[17] Y. M. Sheu, S. A. Trugman, Y.-S. Park, S. Lee, H. T. Yi, S.-W. Cheong, Q. X. Jia, A. J. Taylor, and R. P. Prasankumar, Appl. Phys. Lett. **100**, 242904 (2012).

[18] S. Y. Smolin, M. D. Scafetta, G. W. Guglietta, J. B. Baxter, and S. J. May Appl. Phys. Lett. **105**, 022103 (2014).

[19] D. Talbayev, Jinho Lee, S. A. Trugman, C. L. Zhang, S.-W. Cheong, R. D. Averitt, A. J. Taylor, and R. P. Prasankumar, Phys. Rev. B **91**, 064420 (2015).

[20] K. I. Doig, J. J. P. Peters, S. Nawaz, D. Walker, M. Walker, M. R. Lees, R. Beanland, A. M. Sanchez, C. F. McConville, V. R. Palkar and J. Lloyd-Hughes, Sci. Rep. **5**, 7719 (2015).

[21] M. Pohl, V. V. Pavlov, I. A. Akimov, V. N. Gridnev, R. V. Pisarev, D. R. Yakovlev, and M. Bayer, Phys. Rev. B **88**, 195112 (2013).

[22] Z. Jin, H. Ma, D. Li, G. Ma, M. Wang and C. Zhao, J. Appl. Phys. **109**, 073109 (2011).

[23] A. V. Kimel, F. Bentivegna, V. N. Gridnev, V. V. Pavlov, R. V. Pisarev, and Th. Rasing, Phys. Rev. B **63**, 235201(2001).

[24] R. V. Pisarev, A. S. Moskvin, A. M. Kalashnikova, and Th. Rasing, Phys. Rev. B **79**, 235128 (2009).

[25] X. S. Xu, J. F. Ihlefeld, J. H. Lee, O. K. Ezekoye, E. Vlahos, R. Ramesh, V. Gopalan, X. Q. Pan, D. G. Schlom, and J. L. Musfeldt, Appl. Phys. Lett. 96, 192901 (2010).

[26] C. Degenhardt, M. Fiebig, D. Fröhlich, Th. Lottermoser and R.V. Pisarev, Appl. Phys. B, **73**, 139 (2001).

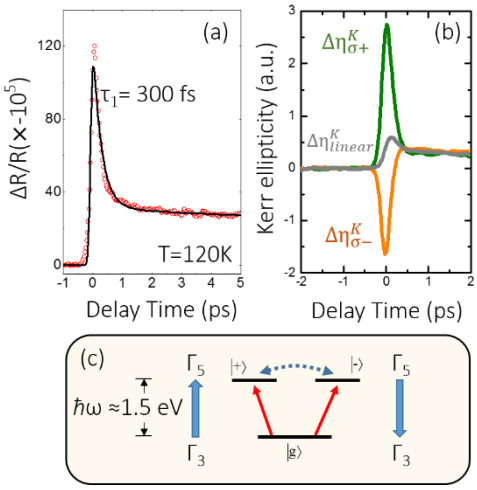

Fig. 1 (a) The transient reflectivity at 120 K for BFMO film. The points are the experimental data and the solid line is a double exponential fitting for the data. (b) Typical photo-induced Kerr ellipticity responses to linearly polarized light ($\Delta\eta^{K}_{linear}$), right ($\Delta\eta^{K}_{\sigma+}$) and left ($\Delta\eta^{K}_{\sigma-}$) circularly polarized light pumping with zero external applied field, measured at room temperature. (c) Schematic energy-level diagram for the dipole allowed transition $\Gamma^3 \rightarrow \Gamma^5$ (solid arrows) between the hybridized $O^{2-}(2p)$-$Mn^{3+}(3d)$ state and the $Mn^{3+}(3d)$ states, ($|g\rangle$ is the ground state and $|+\rangle$, $|-\rangle$ are the degenerate excited states.

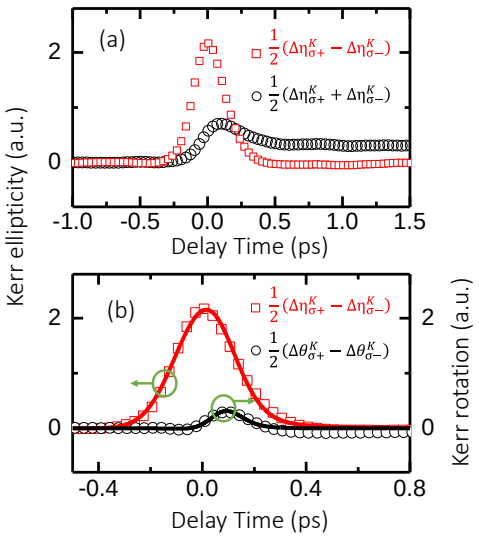

Fig.2 (a) The sum and difference of the transient ellipticity changes excited with right (σ_+) and left (σ_-) circularly polarized pump pulse. (b) The differences of transient MO Kerr ellipticity and rotation changes excited with opposite circularly polarized pump pulse, respectively. The solid lines are the fitted curves.

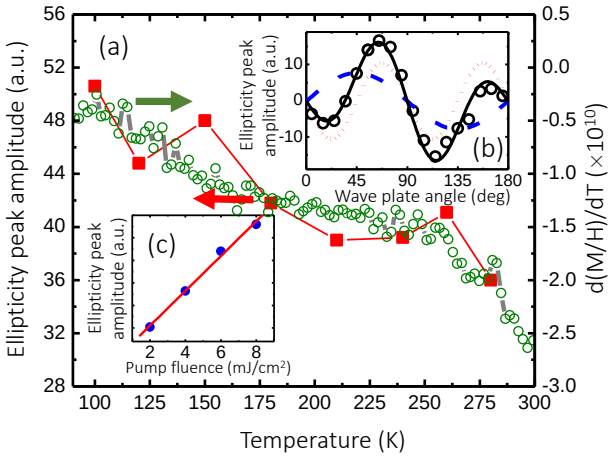

Fig.3 (a) The peak intensity of $\frac{1}{2}\left(\Delta\eta^{K}_{\sigma_+} - \Delta\eta^{K}_{\sigma_-}\right)$(red squares) and the d(M/H)/dT curve (green circles) as a function of temperature in the range from 300 to 100 K. (b) Ellipticity peak amplitude changes as a function of the wave plate angle Φ, and (c) pump fluence dependences of the ellipticity peak amplitude of $\Delta\eta^{K}$ under σ_+ excitation.